DESCRIPTION OF A RADAR CROSS SECTION PREDICTION CODE WITH APPLICATIONS TO INDUSTRIAL PROBLEMS

Francesco Zacca', Giuliano Bettini, Riccardo Cioni
- IDS Ingegneria Dei Sistemi S.p.A., Pisa, Italy -

1) SUMMARY

Following the recent advances in the fields of electromagnetic prediction theory and computer power, and a growing interest to low observables or stealth platforms [1], new software tools for the calculation of radar backscattering have been developed in several companies/institutions. While the basics of the algorithms used are the same, each code has been focused on different ranges of frequencies, kinds of platforms, and so on. This paper describes the prediction code developed at IDS, which is currently used in consultancy activities in the fields of design of new platforms with reduced/controlled RCS, as well as evaluation of the radar signature of existing systems.

2) INTRODUCTION

The RCS prediction procedure mainly consists of three steps (see figure 1): i) modeling; ii) backscattered field computation; iii) data processing.

3) MODELING

The numerical electromagnetic (EM) model of the target approximates the geometrical shape of the target, by decomposing it in a set of simpler shapes covering its surface. The simple shapes are chosen for an easier calculation of the backscattered field. An electromagnetic modeling procedure mainly consists of two steps:

i. Transfer to the computer of the geometry of the target. This may be done through the Acquisition of a set of target coordinates manually or from a digitizer. If a geometrical model created with one of the many commercially available mechanical CAD programs is already existing, it can be automatically adapted to the electromagnetic solver using a software interface.

ii. Meshing, i.e. covering the geometrical model with a set of patches approximating its shape.

These operations are carried out with the help of a tridimensional (3-D) electromagnetic Computer Aided Design (CAD) software.

Modeling may sometimes introduce spurious discontinuities into the model. Possible solutions to this problem are: reduction, whenever possible, of the geometrical discontinuities by a mesh refinement; use of PTD (see later). For each part of the target, the electromagnetic model contains information about its composition, in terms of dielectric and magnetic properties. Dielectric parts increase the complexity of the electromagnetic model, as what lies behind them must in general be modeled too.

Figure 2 shows an example of medium complexity target. Figure 3 shows a detail of a complex target partially composed of dielectric materials, in which some of the inner structures have also been modeled.

4) BACKSCATTERED FIELD CALCULATION

Backscattering problems may be divided in three classes, as a function of target dimensions in terms of wavelengths: i) low frequency region; ii) resonance region; iii) high frequency region. In each region, a different electromagnetic solver has been developed, based on the most suited prediction technique.

4.1) Low Frequency And Resonance Region Solver

The most appropriate electromagnetic prediction technique in this frequency region is the Method Of Moments, MOM, which has been implemented for computing the RCS of a target modeled as a composition of triangular patches [2,3]. As is well known, MOM computes with good precision the backscattered field, taking into account all the scattering phenomena. The problem is that, due to numerical problems, the size of the target must be small in terms of wavelengths.

4.2) High Frequency Solver

There are several prediction techniques for high frequencies [4,5,6]. At present, there are different solvers which implement the following capacities:

a) PO, Physical Optics, for metallic bodies [7].

b) PO extended to dielectric objects [8]. It is possible to model multilayer generic materials, with both electric and magnetic properties [4,9].

c) PTD, Physical Theory of Diffraction, implemented in various forms [10,11,12]: i)ILDCs, from Mitzner, [13,14]; ii)fringe currents, from Michaeli [15]; iii)heuristic formulation, from Sunahara [16].

PO is a computationally efficient technique, and usually gives acceptable prediction results on complex structures with a large number of specular reflectors, such as ships. When targets are observed near grazing incidence, however, PO gives an underestimate of the real backscattered field. As an example, figure 4 shows the RCS polar plot of a flat plate computed with PO and PTD: at angles near normal incidence (about +/-30, for a 20 cm plate at 10 GHz), PO gives acceptable results; at higher angles wedge contributions (also shown on the graph), which can be computed with PTD techniques, become the major sources of backscattering. This is a general behaviour: very low RCS values predicted by PO (in specific directions for particular targets) are usually underestimated. In a complex model, there may arise uncertainties in phase information, which produce uncertainties in peaks and nulls position. This problem can be approached in a statistical way [17]: however, the RCS trend, especially after statistical processing, is not seriously affected by this kind of uncertainties. There are some common characteristic to the various solvers:

- Geometrical masking is accomplished automatically.
- Multiple reflections are automatically located by means of ray tracing techniques. The prediction techniques are implemented in bistatic form, so that multiple reflections can be calculated [18]. The first (n-1) reflections are calculated using GO, while the last n-th is calculated using PO integration.
- There is an option for computing the multipath propagation factor on curved earth, to be used in modifying the predicted electromagnetic field. This yields

what some call the "effective RCS", i.e. the product of the free space RCS and the fourth power of the one-way field pattern propagation factor.

- Backscattered field values can also be computed at finite distance, in the sense that the predicted far field components of each element are vectorially summed taking into account the distance of each element from the observation point (these rays are not parallel at finite distance).

Additional dedicated solvers have been created for the solution of particular scattering problems related to re-entrant structures such as rectangular, circular and arbitrary cavities [19,20,21,22]. The output from the solver is a file containing normalized backscattered electric far field complex values, to be used in the subsequent processing. There are several options of parametric scan: RCS versus one scan angle; RCS versus two scan angles; RCS versus frequency; Range-cross range imaging scan; Azimuth-elevation cross range imaging; "Effective RCS" versus range.

4.3) The Intermediate Region

The methods for high frequencies and low frequencies can be extended towards their limits of applicability so that there is a certain overlap between them. In doing this, it is especially useful to use the PTD.

The results must be analyzed and cross-checked as much as possible, in these applications. In other terms, this is a kind of problem which requires particular attention and must be managed by a skilled electromagnetic engineer [2].

5) DATA PROCESSING AND PRESENTATION

Various post processing algorithms have been implemented. To list some, we have: Fourier direct and inverse transform (unfocused imaging); focused imaging; computation of the electromagnetic center of a target; translation of a radar image in the transformed domain; filtering in space and/or frequency and angle; zero padding; interpolation; arithmetic operations between field maps; statistical processing.

The main processing algorithms can be grouped in three categories:

A) *DATA REDUCTION.*

a' Usually, even the simplest form of RCS data presentation, i.e the azimuth polar plot, is the result of some data reduction processing. The RCS value plotted for each azimuth angle is the result of a statistical processing on a solid angle in both azimuth and elevation. Angular sampling steps are chosen as a function of target cross dimension and wavelength. Statistical processing may be averaging or percentile. Often polar plots of the 10, 50, 90 percentile values are presented in the same chart.

B) *HIGH RESOLUTION IMAGING.*

Given a proper set of complex RCS data computed for different frequencies, a pulse compression high range resolution processing produces high range resolution monodimensional radar images of target RCS as a function of range. In a similar way, given a proper set of complex RCS data computed for different aspect angles, an Inverse Synthetic Aperture Radar (ISAR) signal processing produces high cross-range resolution. Also, pulse compression and ISAR processings can be combined to produce bidimensional high resolution

radar images [23,24,25].
Thus, a high resolution bidimensional radar image can be obtained for each aspect and frequency of interest. The main advantage of this image is the immediate location and quantification in terms of RCS value of the most important scattering centers. In the high resolution processing, a sidelobe suppression window may be used, in order to increase the image dynamic range. Figure 5 shows an example of bidimensional high resolution image.

C) *GRAPHIC UTILITIES.*
There are graphic routines for 1-D cartesian and polar plots, 2-D contour level and waterfall plots. These routines may be used on several kinds of graphic terminals and workstations.

6) VALIDATION

The RCS prediction codes previously described have been validated in various occasions, through:

- Comparison of predictions with measurements available in literature, for canonical shapes.
- Cross comparison of predictions performed with different electromagnetic techniques.
- Comparison with experimental measurements.

We include some examples of comparisons between RCS measurements and/or predictions available in literature and the RCS predictions made with IDS codes. These examples can be grouped as follows:

A) Simple shapes:

A1) Circular cylinder (figure 6).
Measurement in anechoic chamber and PTD prediction from [26,27,28]. Cylinder height 60 cm; base diameter 30 cm; frequency 10 GHz; vertical polarization. Both unidimensional polar plots and bidimensional range-cross range images were obtained, showing excellent agreement between measurements and predictions.

A2) Cone (figure 7).
Measurement from Keys and Primich [9], PTD prediction from [12]. Cone half aperture 40°; base diameter 4.88 wavelengths; horizontal polarization. It is worth noting that the agreement between measurement and PTD prediction is excellent down to rather low frequencies.

B) Medium complexity shapes:

B1) Rectangular cylinder (figures 8a and 8b).
Measurement from [29], PTD prediction from [10]. Geometrical and electrical data shown on the figure.

B2) Frustrum (figures 9a and 9b).
Measurement from [29], PTD prediction from [10]. Geometrical and electrical data shown on the figure.

B3) Hexaedron (figures 10a and 10b).
Measurement from [16], PTD prediction from [30]. Geometrical and electrical data shown on the figure.

C) Multiple reflections effects:

C1) Trihedral corner reflector (figure 11).
The sides are perpendicular and with triangular shape (33 cm leg). Measurement from [9], prediction from [31] Electrical and scan data shown on the figure.

C2) Dihedral non-orthogonal corner reflector (figure 12).
The two faces are identical, 5 wavelengths large, 10 wavelengths high, the corner angle is 600, polarization is vertical. Measurement from [32], prediction from [31].
As shown from the above examples, calculations of more than two reflections yields much better results. In the codes there are options for computation of n-th order reflections.

D) Cavities:

D.1) Simple cylindrical cavity (figure 13).
Reference prediction from [33], IDS modal prediction from [31]. Base diameter 20 cm; length 60 cm; frequency 10 Ghz; horizontal polarization.

D2) Complex "S" shaped cavity (figure 14).
Reference prediction from [34], IDS prediction from [31]. Normalized frequency plot, see [34] for geometrical details.

E) Dielectric materials:

E1) Dielectric disks (figures 15a and 15b).
Measurement from [35], prediction from [8]. Geometrical and electrical data shown on the figure.

7) APPLICATIONS

The RCS prediction codes have been used for several applications on various kinds of platforms, such as aircraft, helicopters, missiles, ships, tanks. They have proven to be a cost-effective solution as a support to measurements in the assessment of RCS levels of existing platforms. Also, prediction is surely the only available technique in the preliminary design of new platforms. At this stage of design it is now possible to analyze the various design options in terms of their effect on the radar signature, so that effective reduction solutions can be defined and applied since the earliest design phases.

8) CONCLUSIONS

RCS prediction is a mature art, which can be applied to industrial problems with high levels of confidence in a very cost-effective way. Theoretical work is always continuing, producing ever more accurate and powerful codes, capable of performing well on complex shapes. Prediction is however a complex art, and must be applied with a deep understanding of the electromagnetic theory it is based on. With these assumptions, prediction can be a valuable and in some cases unique tool in the design and evaluation of reduced/controlled RCS platforms. Also, theoretical prediction should always serve as a companion for measurements.

9) BIBLIOGRAPHY

[1] F. Bessi, F. Zacca': "Introduction To Stealth: Radar Cross Section And The Design Of Reduced/Controlled RCS Platforms", Military Technology, May 1989.

[2] A. Bicci, R. Cioni, F. Zacca': "Study Of RCS In The Intermediate And Low Frequency Region", IDS internal report n. 88/128.

[3] R.F. Harrington: "Field Computation By Moment Methods", MacMillan, 1968.

[4] E.F. Knott, J.F. Shaeffer, M.T. Tuley: "Radar Cross Section", Artech House, 1985.

[5] J.W. Goodman: "Introduction To Fourier Optics", Mc Graw Hill, 1968.

[6] E.F. Knott: "A Progression Of High Frequency RCS Prediction Techniques", IEEE Proceedings, February 1985.

[7] G. Speranza: "Calculation Of The Radar Echo Of A Plane Polygonal Plate With Physical Optics Approximation (in Italian)", IDS internal report n. 85/066.

[8] G. Speranza, P. Milani:"Application Of Physical Optics To Dielectric And Absorbing Materials (in Italian)", IDS internal report n. 86/006.

[9] G.T. Ruck: "Radar Cross Section Handbook", Plenum Press 1970.

[10] G. Speranza: "Analysis Of Methods For Computing Wedge RCS With Equivalent Currents (in Italian)", IDS internal report n. 86/016.

[11] G. Speranza: "Calculation Of Wedge RCS With Surface Impedance Methods (in Italian)", IDS internal report n. 87/060.

[12] A. Bicci, R. Cioni: "Upgrade Of The PTD Code And Validation Of Its Application At Low Frequencies (in Italian)", IDS internal report n. 88/086.

[13] K.M. Mitzner: "Incremental Length Diffraction Coefficients", Technical Report n. AFAL-TR-73-296, Northrop corp., April 1974.

[14] E.F. Knott: "The Relationship Between Mitzner's ILDC And Michaeli's Equivalent Currents", IEEE AP Transactions, January 1985.

[15] A. Michaeli: "Equivalent Edge Currents For Arbitrary Aspects Of Observation", IEEE AP Transactions, January 1985.

[16] Y. Sunahara, S. Kaniya, H. Aoki, S. Sato, S. Mamo: "Backscattering From Triangular Cylinder And Hexaedron", proceedings of the ISAP, 1986.

[17] A.L. Maffett: "Topics For A Statistical Description Of Radar Cross Section", Wiley, 1989.

[18] G. Speranza: "Application Of Physical Optics To The Calculation Of the RCS Of Complex Structures (in Italian)", IDS internal report n. 86/013.

[19] G. Speranza: "Calculation With Physical Optics Of The RCS Of Cavities (in Italian)", IDS internal report n. 87/124.

[20] A. Bicci: "A Computer Code For Calculation Of The RCS Of Rectangular Cavities With Physical Optics (in Italian)", IDS internal report n. 88/062.

[21] R. Cioni: "Estimate Of The RCS Of A Cylindrical Cavity (in Italian)", IDS internal report n. 89/004.

[22] J.W. Crispin, A.L. Maffett: "Estimating The RCS Of A Cavity", IEEE AES Transactions, September 1970.

[23] D.L. Mensa: "High Resolution Radar Imaging", Artech House 1981.

[24] G. Bettini: "Elements Of High Resolution Radar Techniques (in Italian)", Tipografia Editrice Pisana, 1988.

[25] E. Dalle Mese, G. Corsini, G. Manara, G. Bettini, F. Bessi, F. Zacca': "Radar Imaging Of Non-Cooperating Manoeuvering Aircraft", IEEE International Radar Conference, Arlington 1990.

[26] R. Tiberio, G. Pelosi, G. Bettini: "RCS Reconstruction Using Microwave Imaging", Alta Frequenza, March 1989.

[27] B. Audone, G. Bettini, B. Casali, M. Calamia, G. Pelosi, R. Tiberio, G. Manara: "An Application Of Imaging Techniques For Reconstructing The RCS Of Radar Targets", 7th national meeting of applied electromagnetics, Frascati September 1988.

[28] F. Bessi, G. Bettini, G. Pelosi, R. Tiberio: "Radar Imaging For Scattering Mechanism Extraction And Reconstruction", ICEAA, International Conference on Electromagnetics in Aerospace Applications, Torino September 1989.

[29] G.A. Thiele: "Fundamentals Of Radar Cross Section", lectures presented by SCEEE, San Diego 1985.

[30] G. Speranza, B. Casali: "Developments In The Computation Methods Of Wedge RCS With Equivalent Currents (in Italian)", IDS internal report n. 86/091.

[31] R. Cioni: "Characteristics And Performance Of The RCS_PREDICTION Software Package (in Italian)", IDS internal report n. 90/047.

[32] W.C. Anderson: "Consequences Of Nonortogonality On The Scattering Properties Of Dihedral Reflectors", IEEE AP transactions, October 1987.

[33] C.S. Lee, S. Lee: "RCS Of A Coated Circular Waveguide Terminated By A Perfect Conductor. IEEE AP Transactions, April 1987.

[34] P.H. Pathak, R.J. Burkholder: "Modal, Ray, And Beam Techniques For Analyzing The EM Scattering By Open-Ended Waveguide Cavities". IEEE AP Transactions, May 1989.

[35] D.M. Le Vine: "the Radar Cross Section Of Dielectric Disks", IEEE AP transactions, January 1984.

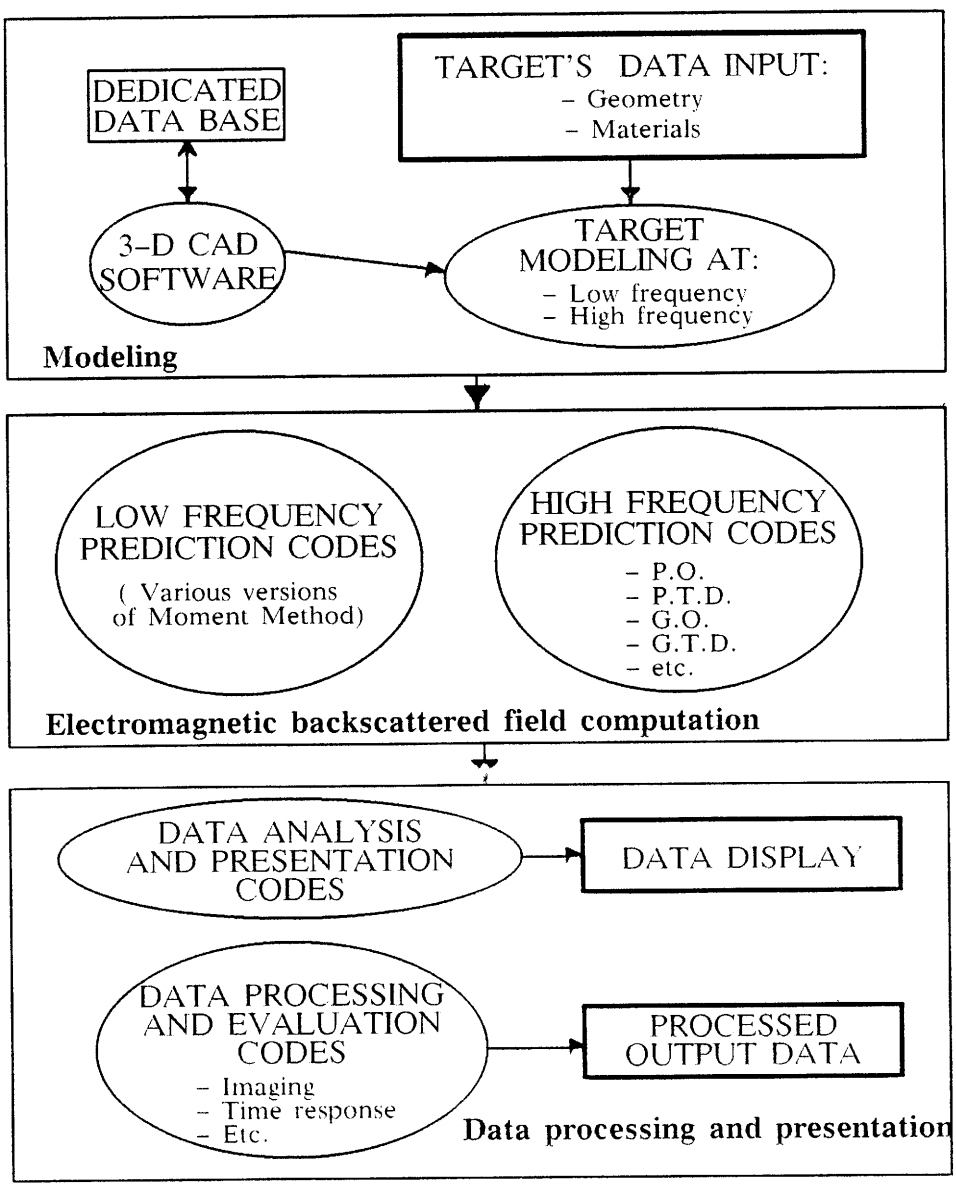

Figure 1: The RCS prediction procedure

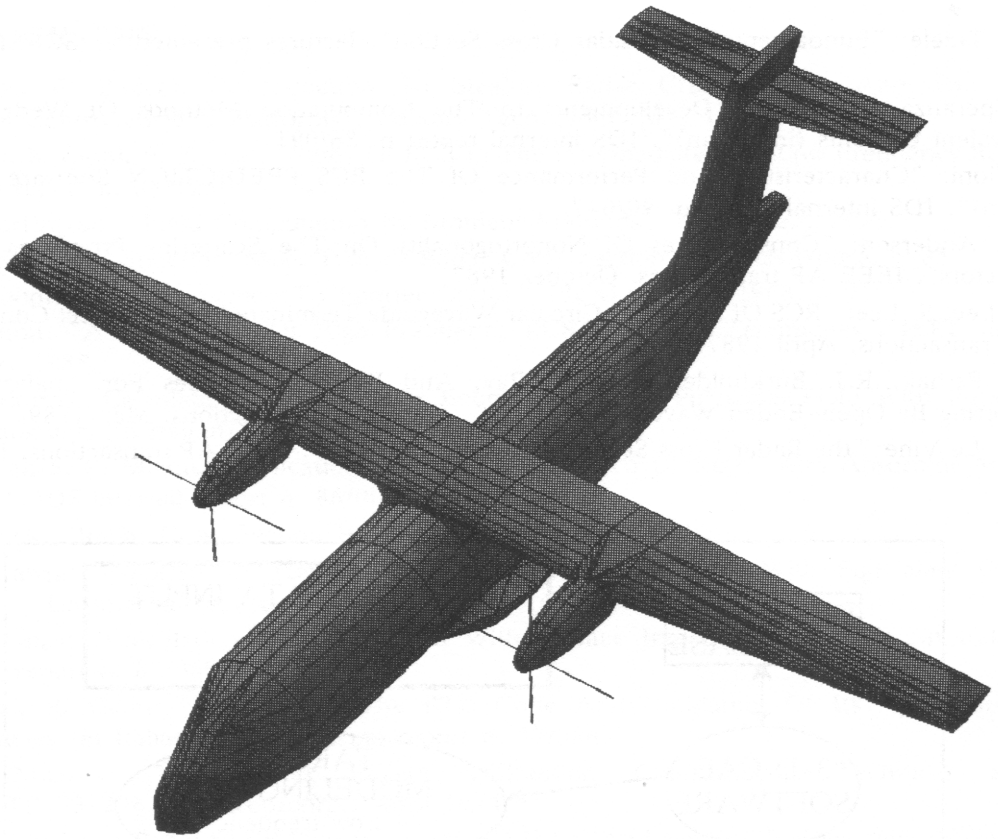

Fig. 2: example of electromagnetic model

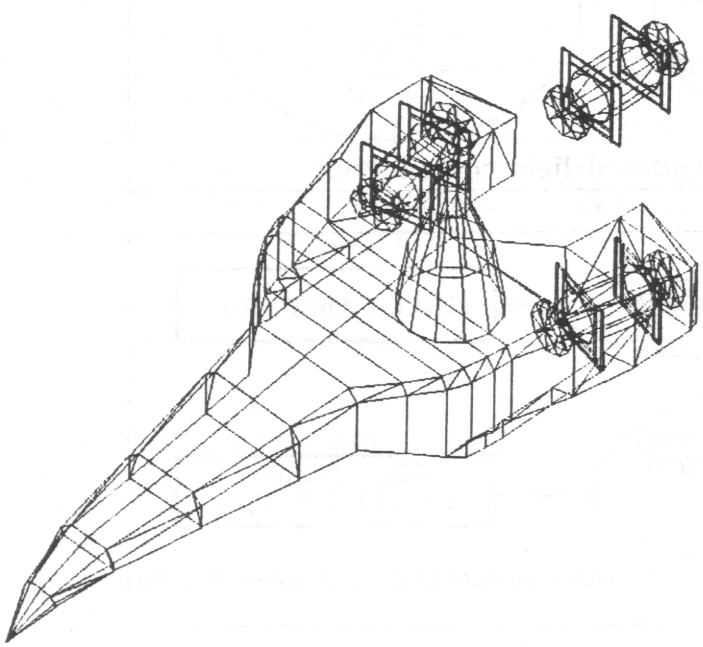

Fig. 3: detail of a complex e.m. model

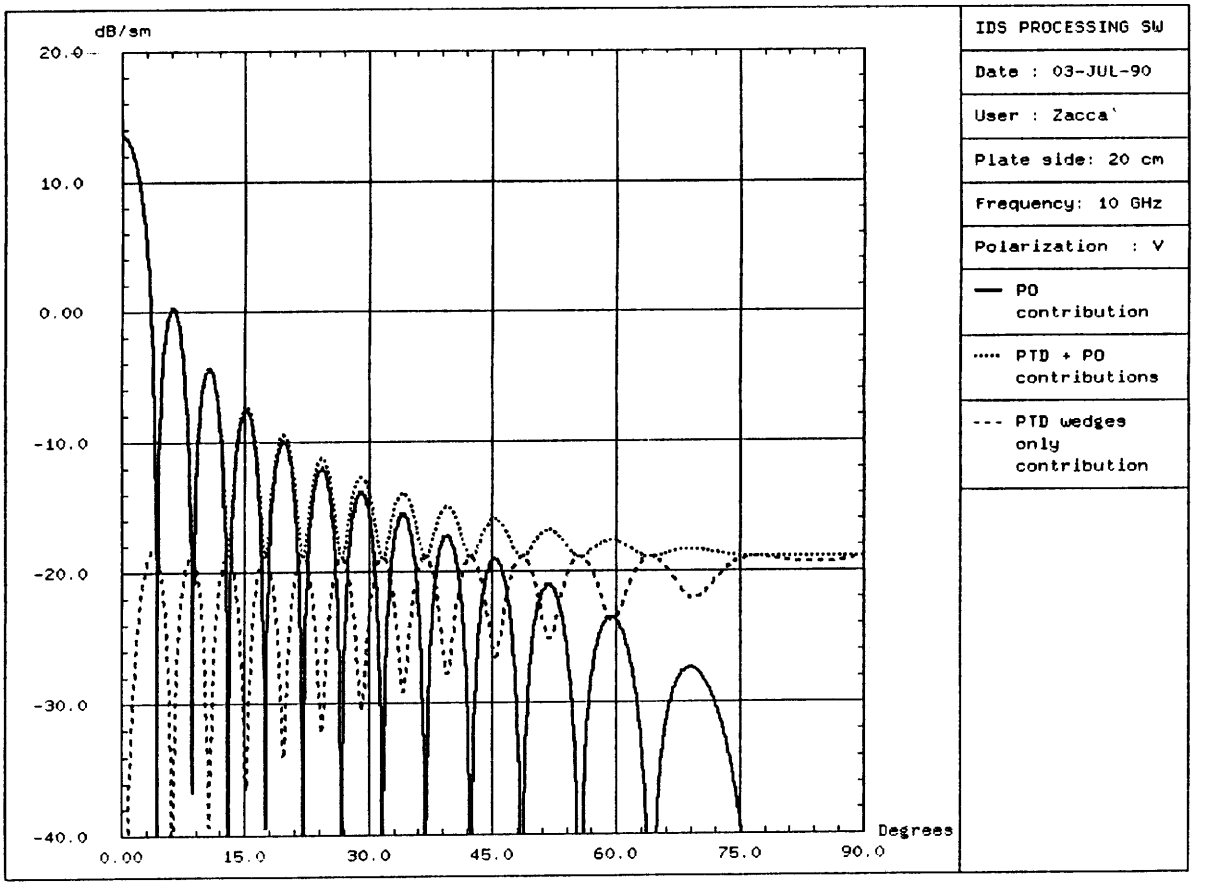

Fig. 4: RCS of a square flat plate

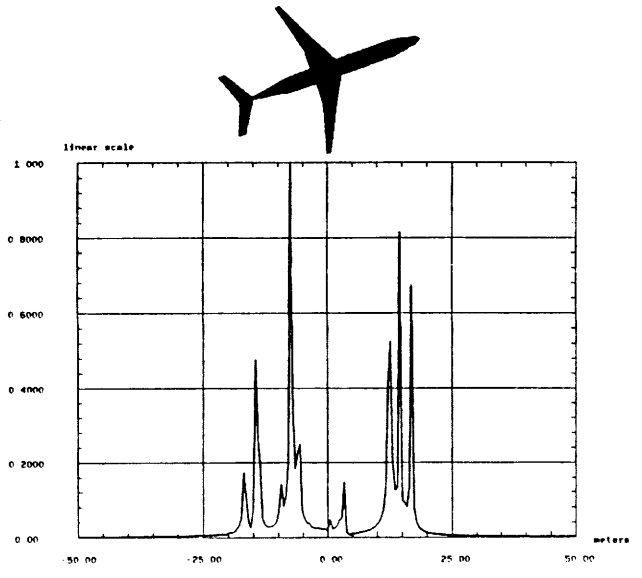

Unidimensional profile with optimum

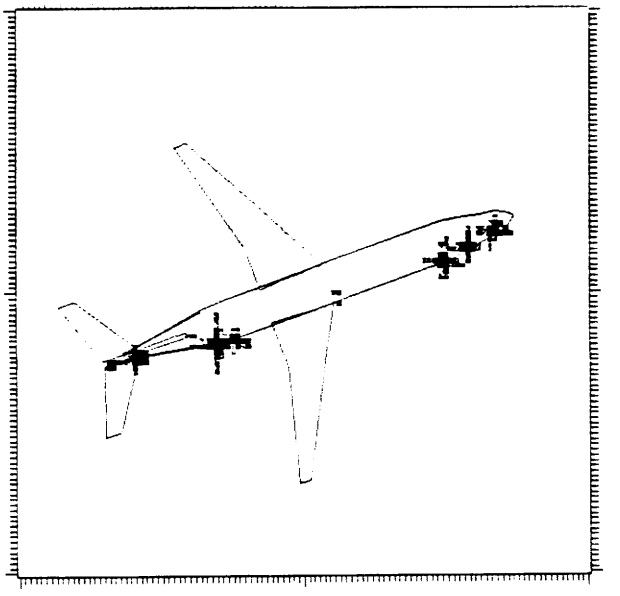

Bidimensional image

Fig. 5

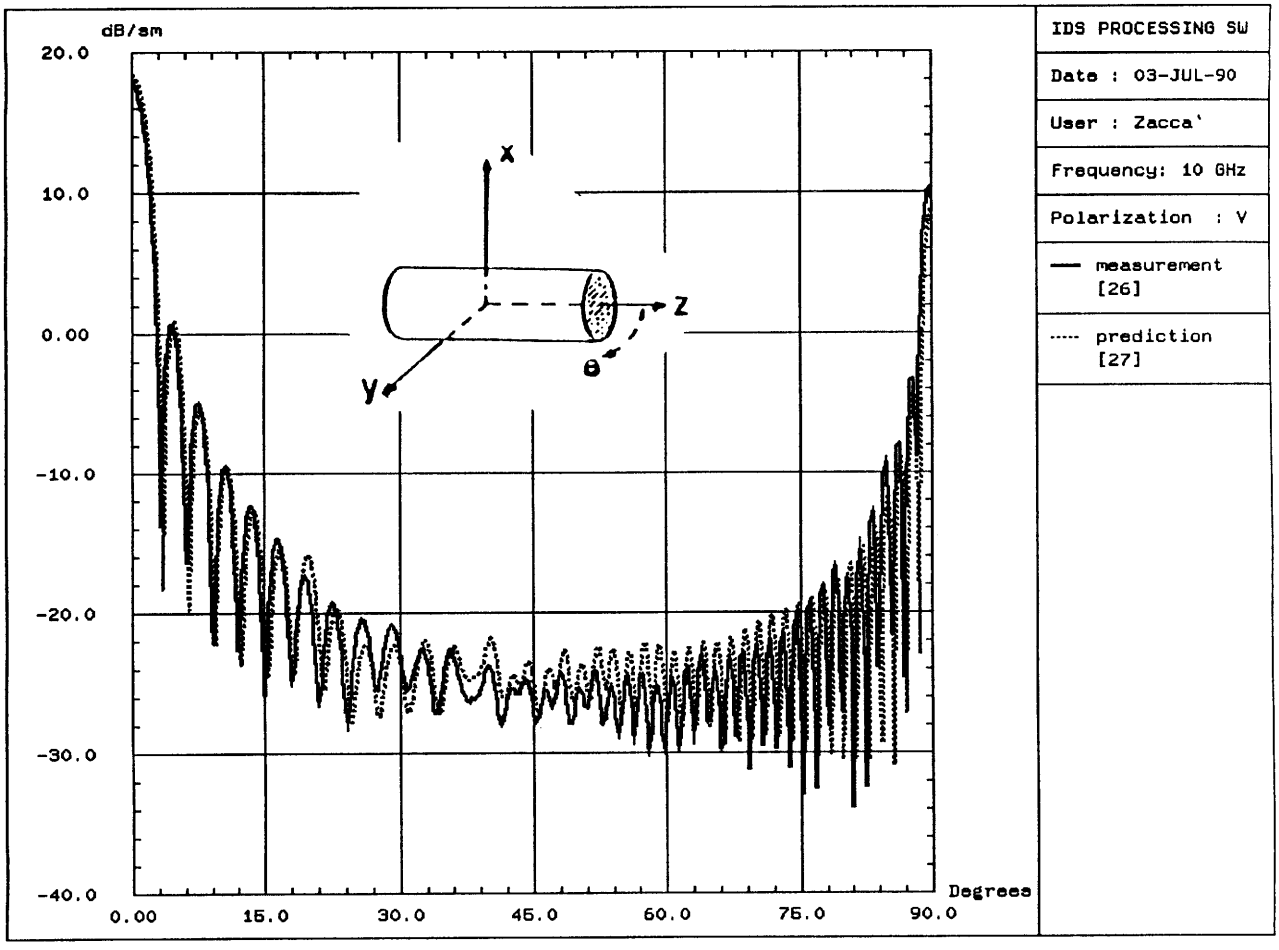

Fig. 6: RCS of a circular cylinder

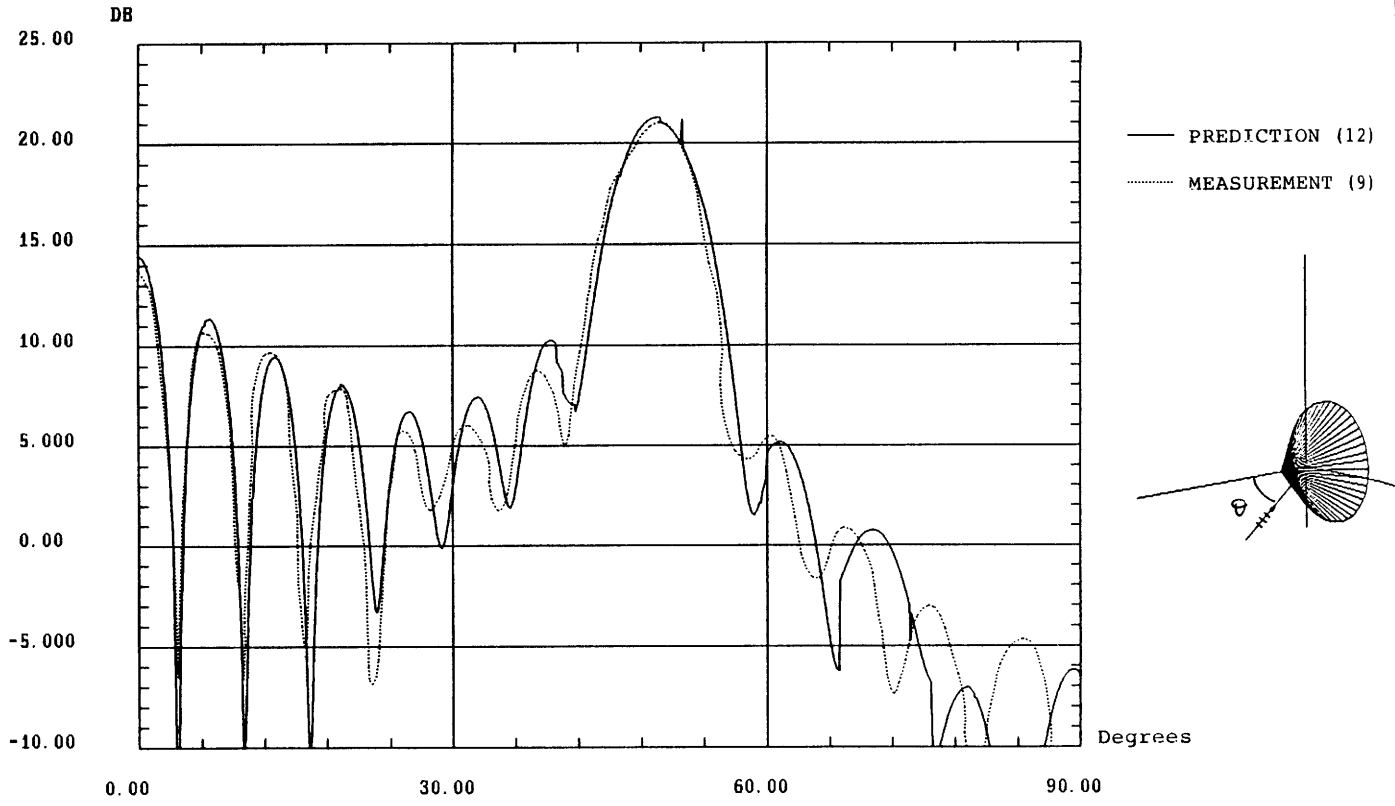

Fig. 7: RCS of a cone

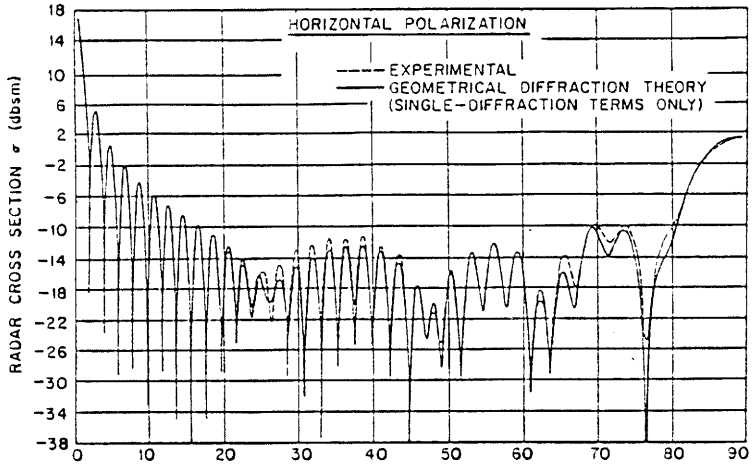

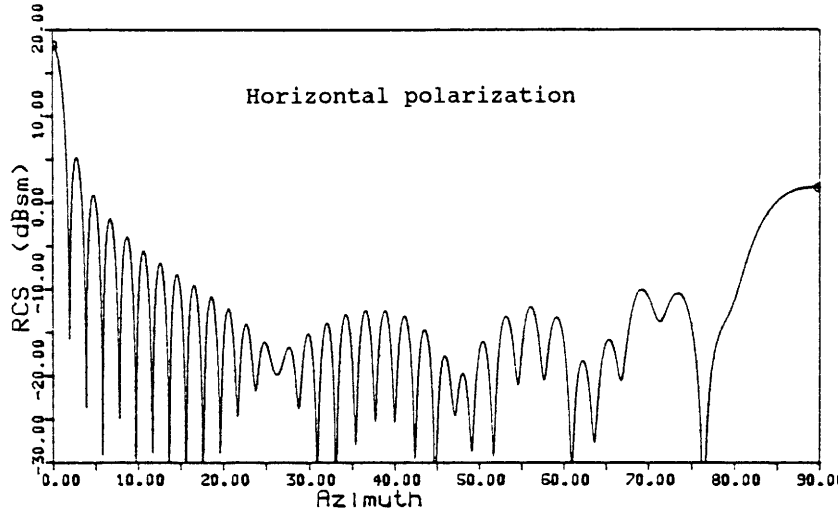

measurement, after Thiele (29)

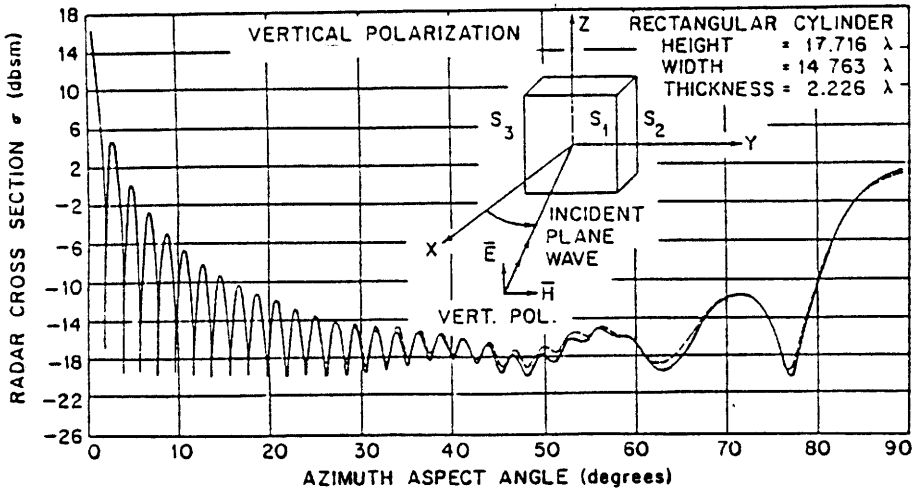

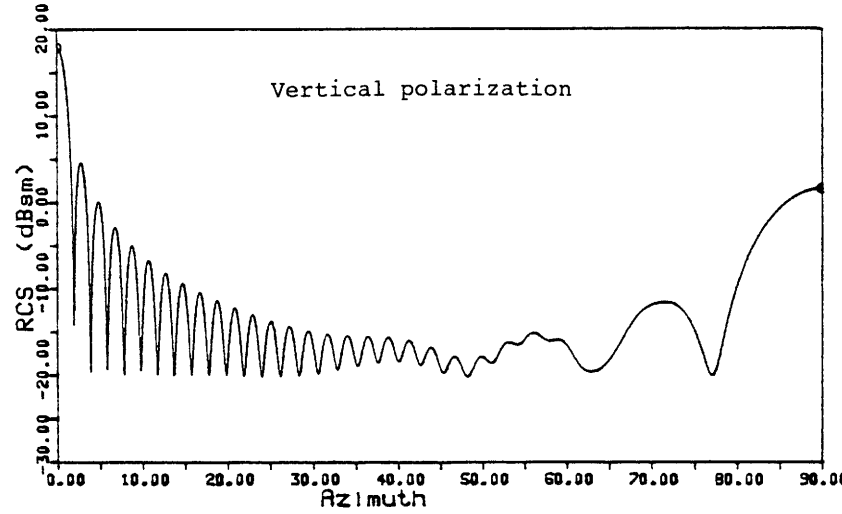

(a) (b)

Fig. 8: RCS of a rectangular cylinder

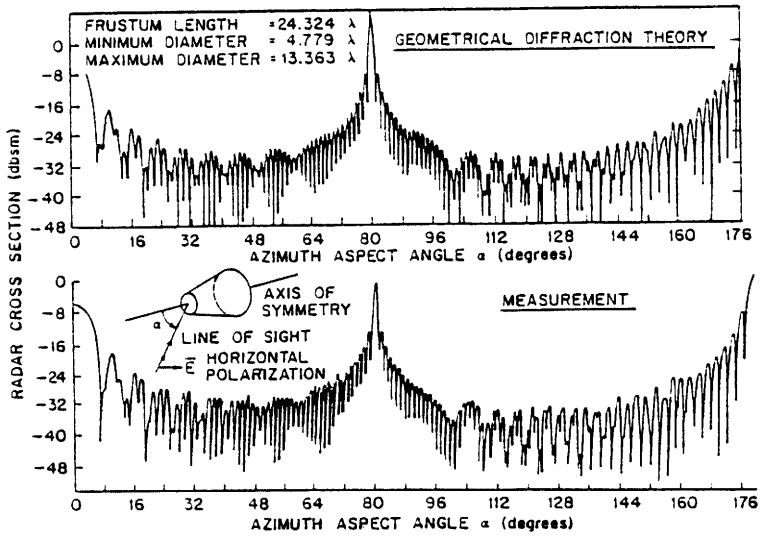

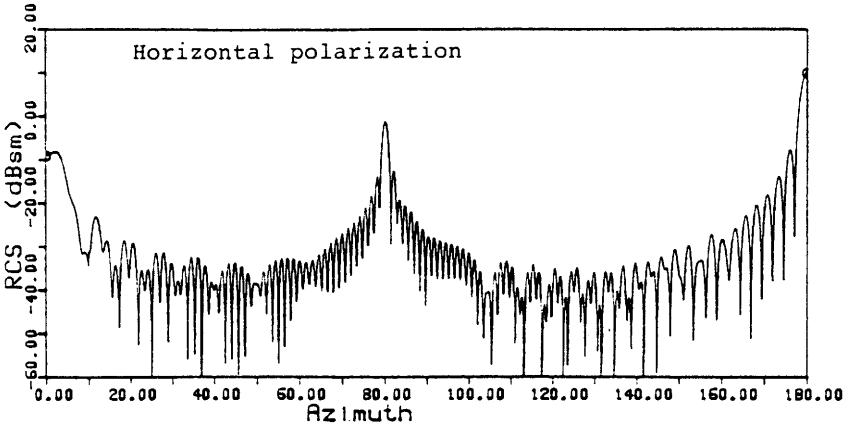

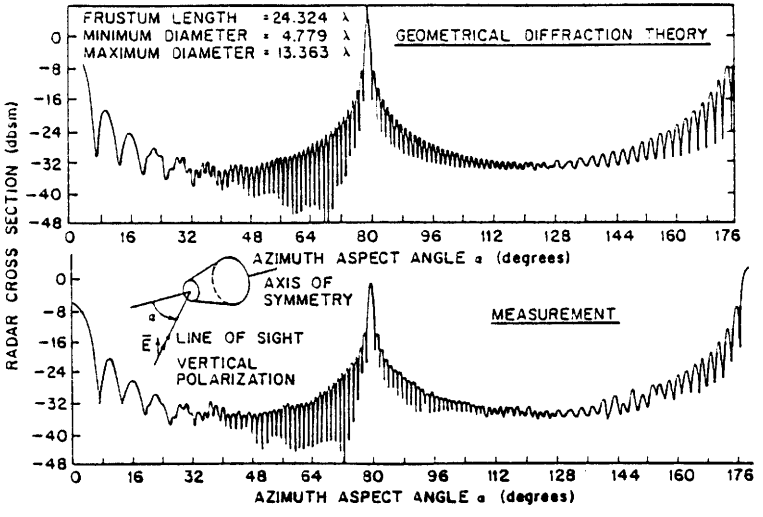

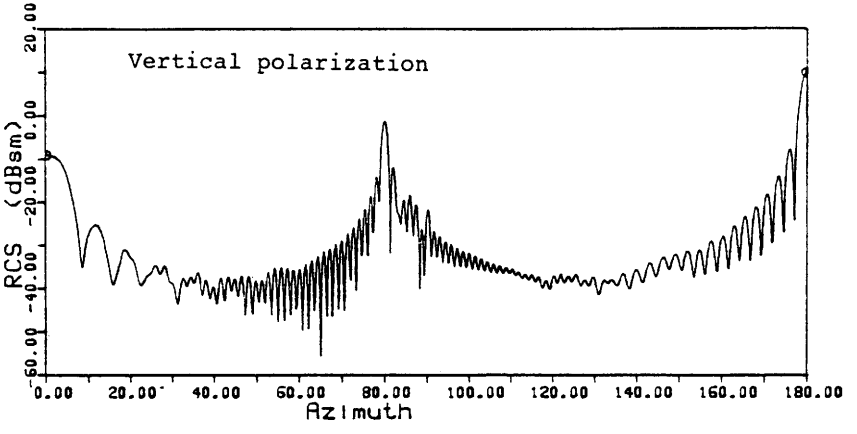

(a) (b)

Fig. 9: RCS of a frustrum

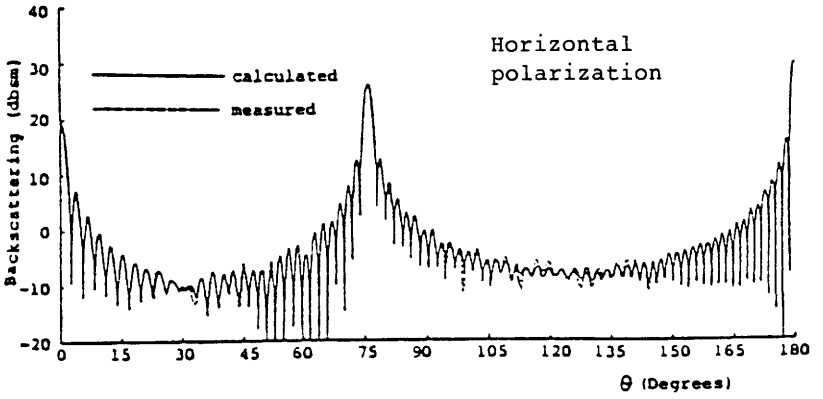

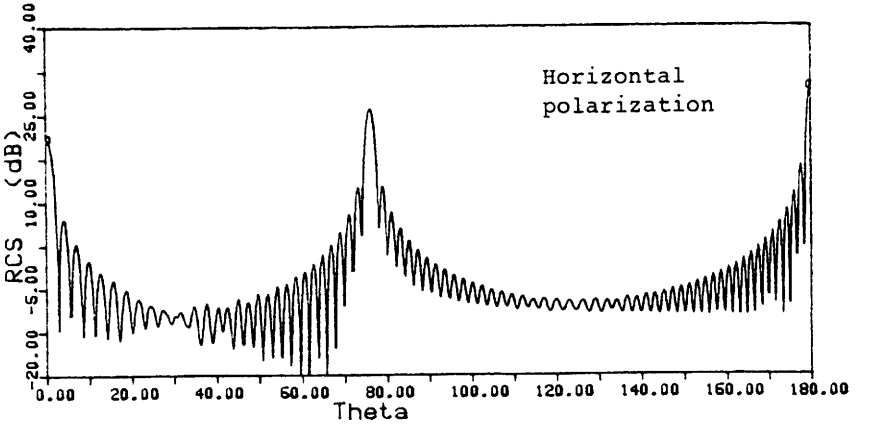

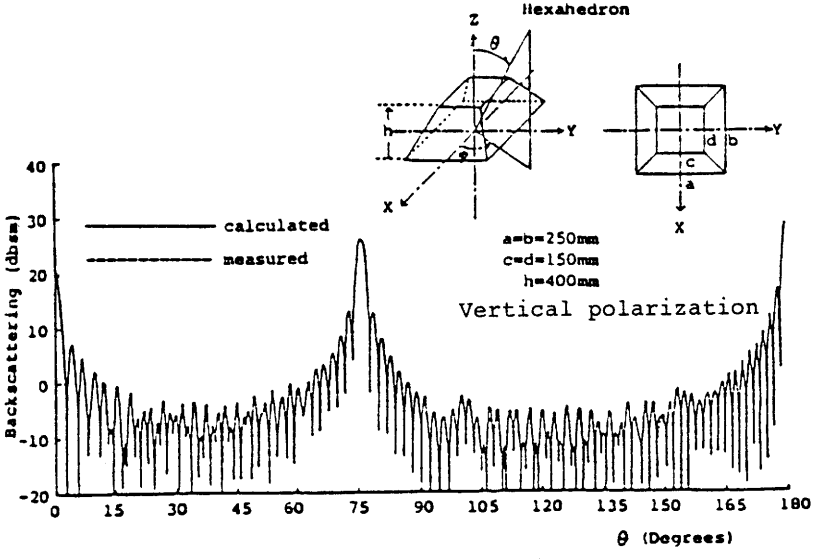

(a): measurement

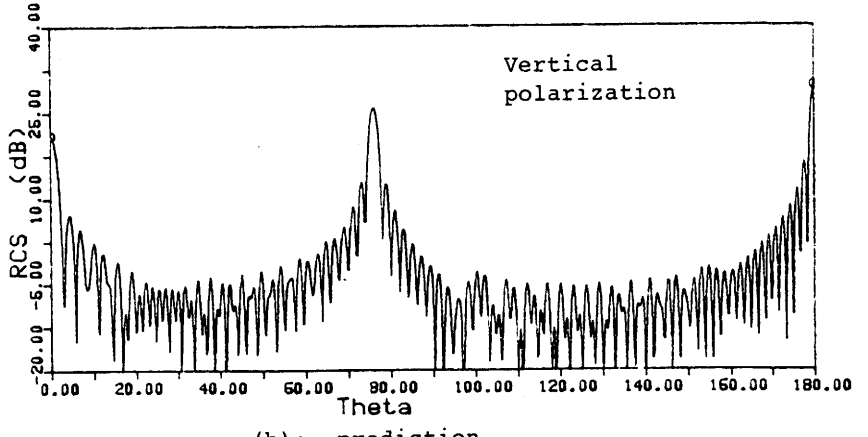

(b): prediction

Fig. 10: RCS of a frustrum

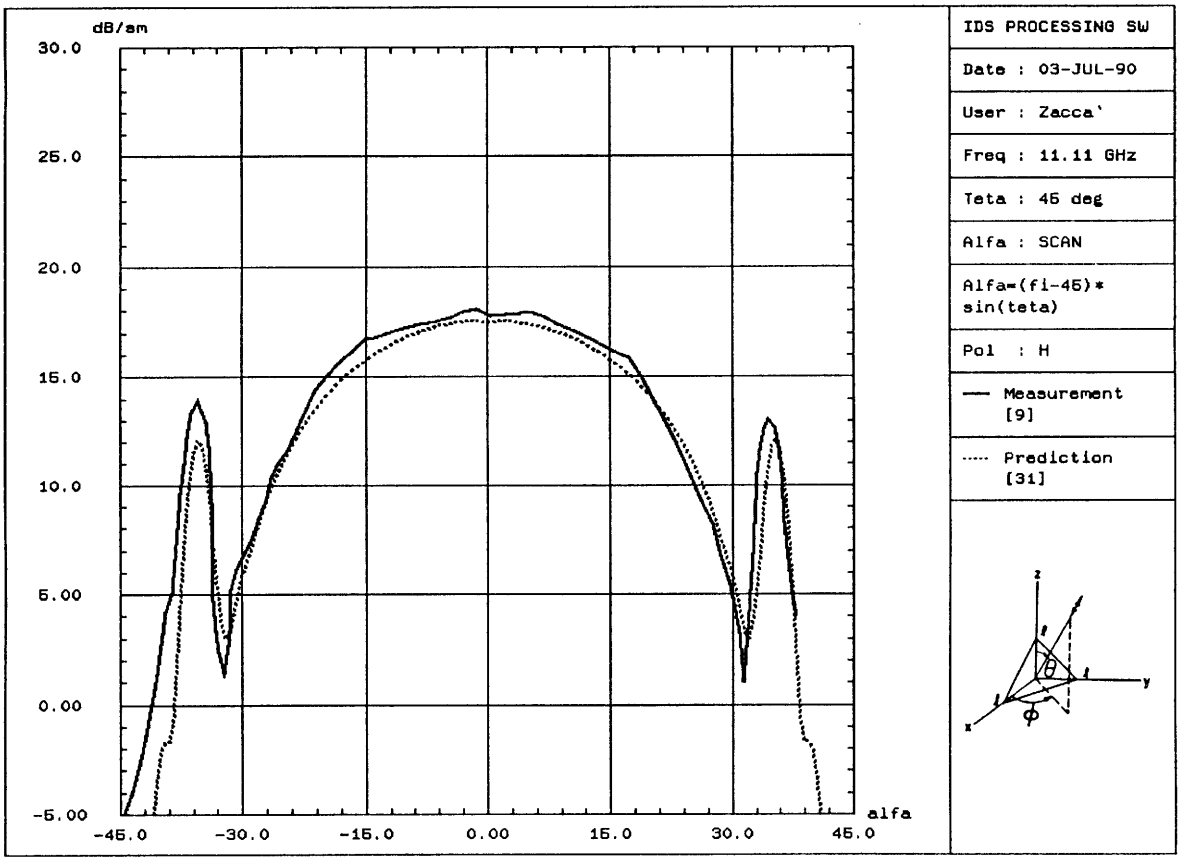

Fig. 11: RCS of a trihedral corner reflector with triangular faces

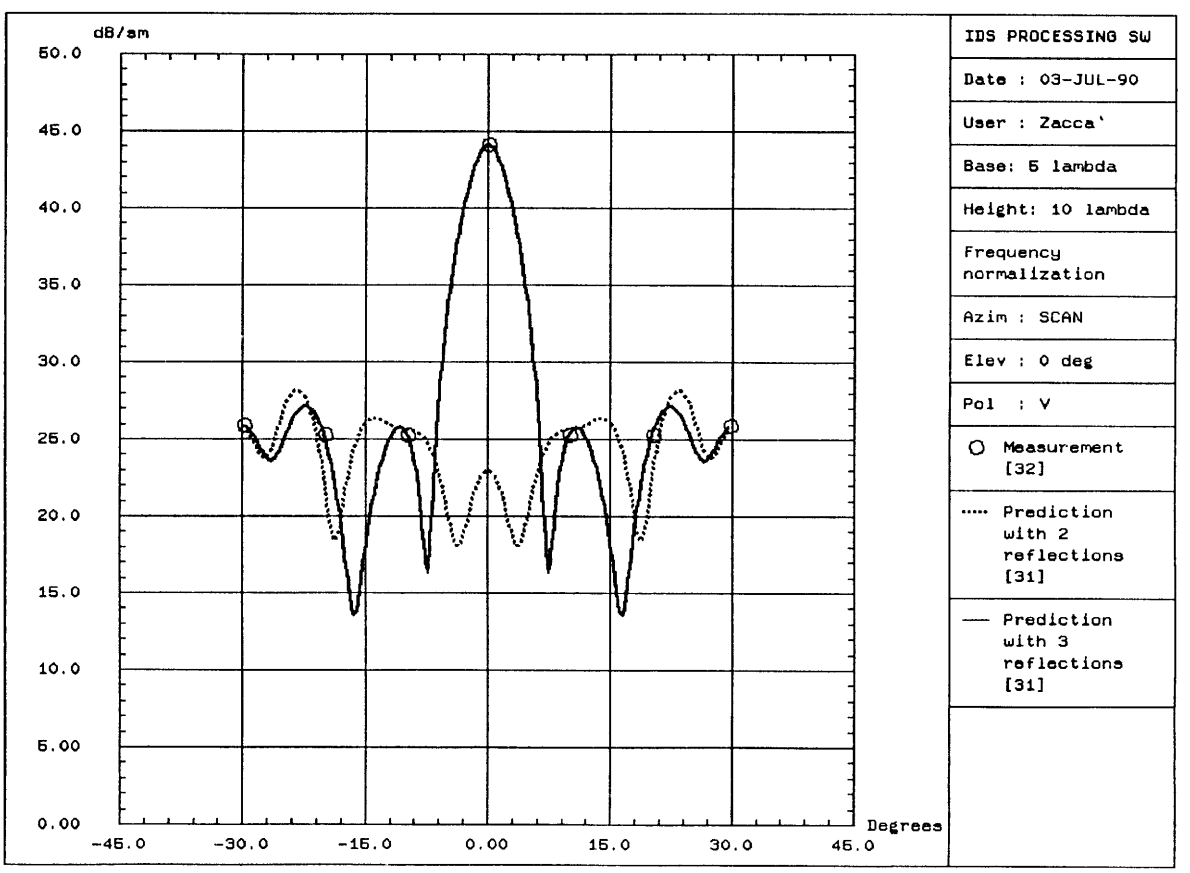

Fig. 12: RCS of a dihedral non-orthogonal corner reflector

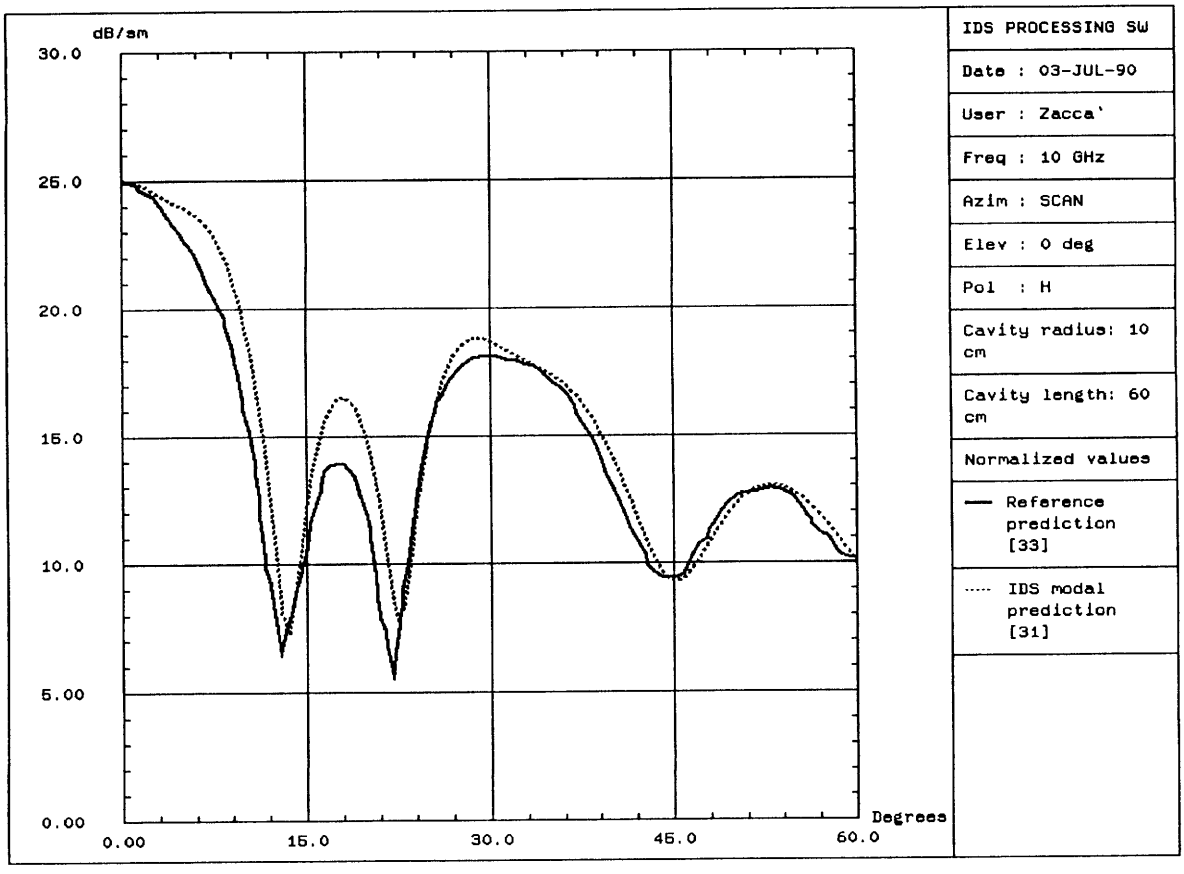

Fig. 13: RCS of a simple cylindrical cavity

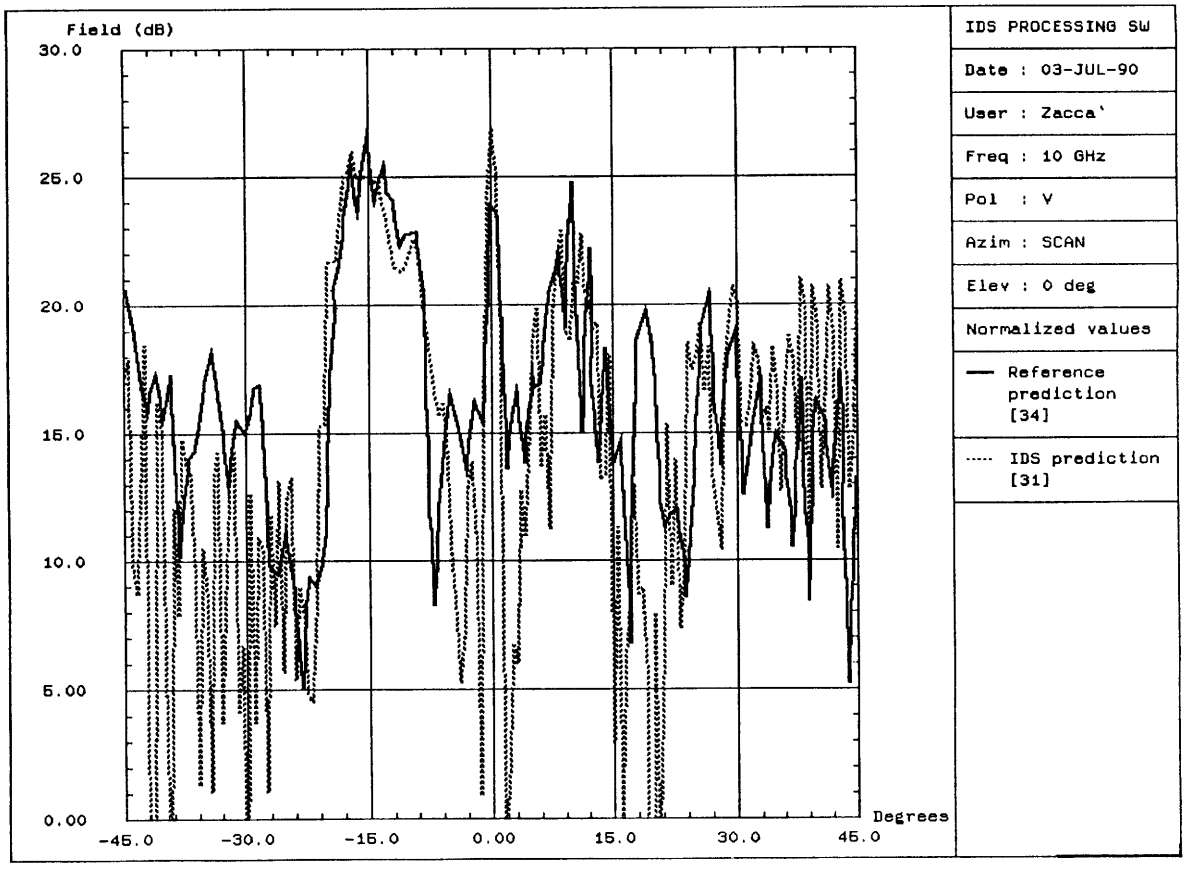

Fig. 14: e.m. field backscattered by a complex "S" shaped cavi

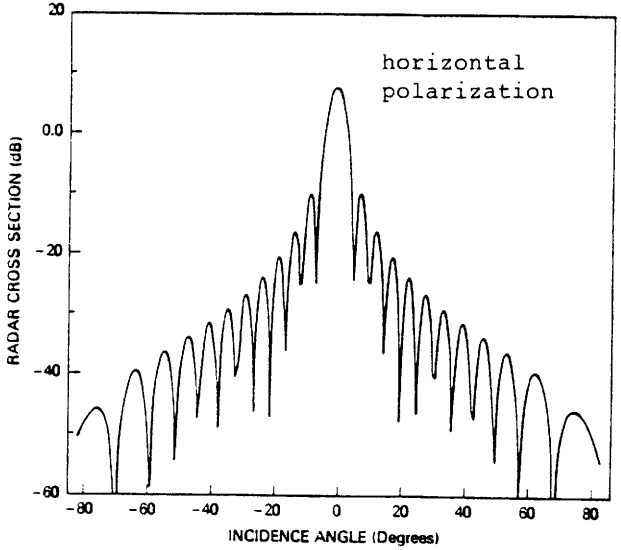

Radar cross section $\sigma_{hh}(\theta)$ for a circular disk with radius a = 10 cm, thickness T = 0.5 cm, relative dielectric constant ϵ_r = 25 + j11, and frequency f = 9 GHz.

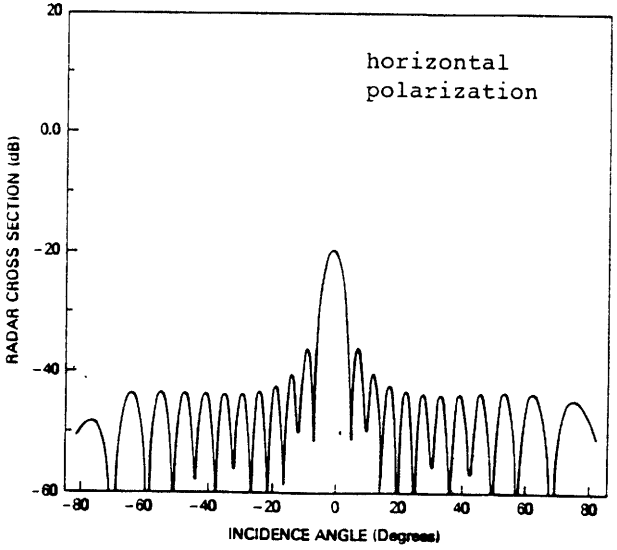

Radar cross section $\sigma_{hh}(\theta)$ of a circular disk one half wavelength thick: radius a = 10 cm, thickness T = 0.5 cm, relative dielectric constant ϵ_r = 11, and frequency f = 9 GHz.

(a): measurement, after LeVine (35)

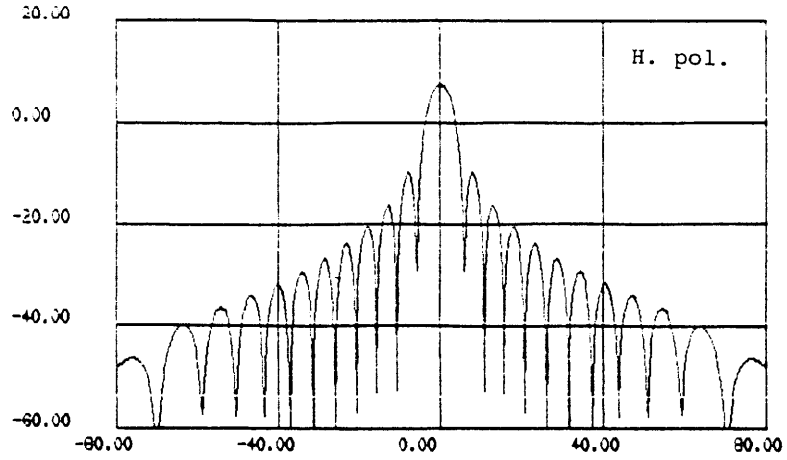

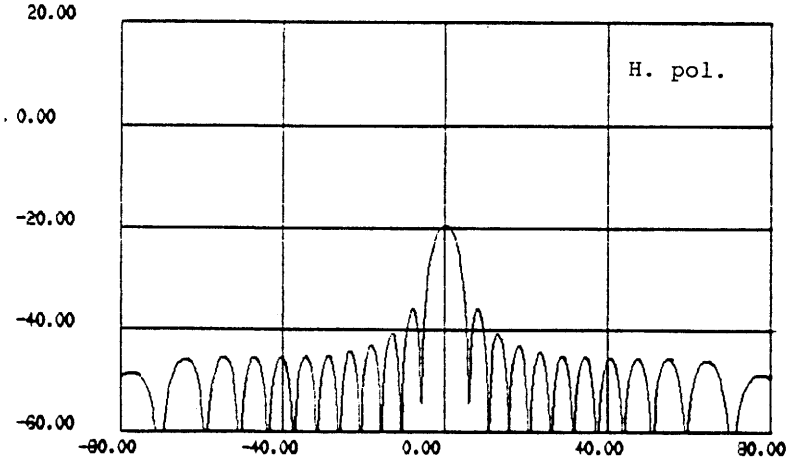

(b): prediction

Fig. 15: RCS of a dielectric circular disk